

Topological Phase Transitions of Dirac Magnons in Honeycomb Ferromagnets

Yu-Shan Lu,¹ Jian-Lin Li,¹ and Chien-Te Wu^{1,2}

¹*Department of Electrophysics, National Yang Ming Chiao Tung University, Hsinchu, Taiwan*

²*Physics Division, National Center for Theoretical Sciences, Taipei, Taiwan*

The study of magnonic thermal Hall effect has recently attracted attention because this effect can be associated with topological phases activated by Dzyaloshinskii-Moriya interaction, which acts similar to a spin-orbital coupling in an electronic system. A topological phase transition may arise when there exist two or more distinct topological phases, and this transition is often revealed by a gap closing. In this work, we consider a ferromagnetic honeycomb lattice described by a Hamiltonian that contains Heisenberg exchange interaction, Dzyaloshinskii-Moriya interaction, and an applied Zeeman field. When expanding the spin operators in the Hamiltonian using Holstein-Primakoff (HP) transformation to the order of $S^{1/2}$, where S is the magnitude of spin, the thermal Hall conductivity stays negative for all values of parameters such as the strength of Zeeman interaction and temperature. However, we demonstrate in this work that by including the next order, $S^{-1/2}$, in HP transformation to take into account magnon-magnon interaction, the Hartree type of interaction gives rise to topological phase transitions driven by temperature. When the temperature increases, we find that the gap of the magnonic energy spectrum closes at Dirac points at a critical temperature, T_c , and the gap-closing is indeed the signature for a topological phase transition as confirmed by showing that the Chern numbers are distinct above and below T_c . Finally, our analysis points out that thermal Hall conductivity exhibits sign reversal at the same temperature. This phenomenon can be used in experiments to verify the topological nature of magnons in honeycomb magnets.

Introduction.— In condensed matter physics, the notion of topological ordered phases has opened new avenues to understand exotic phases of matter that cannot fit into the Landau's paradigm. The integer quantum Hall effect in a two dimensional electron gas is one such example where the time-reversal symmetry is broken and the electronic system is in a topologically ordered phase characterized by quantized Hall conductance. Another prominent example is the discovery of the symmetry-protected topological order in topological insulators [1–3]. While these ordered phases are not classified in the Landau's theory, they can be linked to certain topological invariants. Although the above two examples consider fermions, the topological aspect of bosons has also recently attracted considerable interest, e.g., a symmetry-protected topological phase of ^{87}Rb atoms trapped in a one-dimensional lattice has been realized experimentally [4]. As will be illustrated in this paper, an essential difference between fermionic and bosonic topological orders is the underlying quantum statistics, which causes distinct transport properties associated with topological invariants.

The physics of topological orders in systems consisting of bosonic collective excitations such as magnons in a magnet also draws much attention because of the possibility of nonzero thermal Hall conductivity [5–15]. Unlike electrons, magnons are charge neutral, and thereby not experiencing any Lorentz force. For this reason, topological properties of magnonic systems cannot be studied via the standard Hall effect. Nevertheless, it is shown [16] that in magnonic systems an antisymmetric interaction such as the Dzyaloshinskii-Moriya interaction (DMI), between spin moments plays a similar role as Lorentz force and gives rise to thermal Hall effect.

The theoretical work on the thermal Hall effect induced by an external magnetic field in ferromagnets with particular lattice structures such as kagome lattice was first studied in Ref. [17]. Experimental evidence for the magnonic thermal Hall effect in a ferromagnetic insulator with pyrochlore lattice structure is also reported around the same time [18]. Apart from pyrochlore lattice, experimental results on the thermal Hall effect of Cu(1-3, bdc) with Kagome lattice also reveal a magnon origin [19]. Interestingly, the observed thermal Hall conductivity undergoes an unusual sign reversal either by tuning the magnetic field or temperature in both experimental works [18, 19]. The origin for the sign reversal is also theoretically investigated in Refs. [20, 21] by studying topological properties of kagome ferromagnets. It is found that the changes of the sign are associated with topological phase transitions, while the converse is not necessarily true. Hence a topological phase transition is not always accompanied by a sign reversal of the thermal Hall conductivity.

The thermal Hall effect is also theoretically predicted to exist in honeycomb lattices [22, 23] in addition to widely studied kagome lattices [6, 19, 20, 24]. It is found that Dirac points are gapped as the time reversal symmetry is broken by DMI, similar to the effect of the next-nearest neighbor interaction in Haldane model for electronic systems [25, 26]. In contrast to kagome lattices, the sign of thermal Hall conductivity in honeycomb lattices is predicted in Ref. [23] to never change for all values of relevant parameters such as temperature and applied magnetic field. There, many body interaction effects are not included. Recently, Pershoguba *et al.* [27] considered magnon-magnon interactions in honeycomb lattices and found that these many body interactions lead to a notable

momentum-dependent renormalization of magnonic energy bands. Their theory successfully resolved anomalies in neutron-scattering data for CrBr_3 that had been unexplained for nearly fifty years. It is to be noted that the DMI is not taken into account in their theory, although its presence in honeycomb ferromagnet CrI_3 has recently been experimentally confirmed [28]. From the above discussion, it is clear that both DMI and many body effects play an important role and they cannot be ignored. Therefore, in this paper, we theoretically incorporate DMI and magnon-magnon interactions into our model Hamiltonian to investigate the topological aspect of honeycomb ferromagnets. We find that topological phase transitions in honeycomb ferromagnets indeed can be driven by magnon-magnon interactions and these transitions can be confirmed from thermal Hall measurements. Below we shall first introduce our theoretical formalism and then present our results on topological properties of honeycomb ferromagnets.

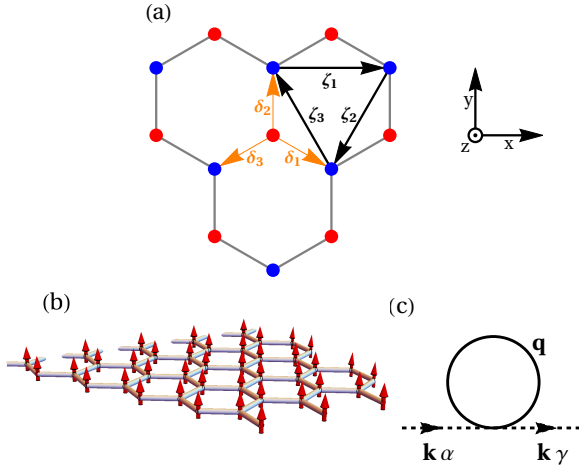


Figure 1. (a) Schematics of a honeycomb lattice. Three nearest-neighbor and next-nearest-neighbor vectors are labeled as δ_i and ζ_i ($i = 1, 2, 3$), respectively. (b) The localized spins are represented by red arrows and point along the z -axis, same as the external magnetic field, in the $T = 0$ limit. (c) The Feynman diagram for the Hartree-type self-energy. Here the Green's functions to be contracted are denoted by the dashed arrows with α and γ denoting the up or down band.

Background theory.—We consider localized spin moments arranged on a honeycomb lattice in the xy plane as shown in Fig. 1(a). The corresponding Hamiltonian associated with these spins reads as

$$H = -J \sum_{\langle ij \rangle} \hat{\mathbf{S}}_i \cdot \hat{\mathbf{S}}_j - J' \sum_{\langle\langle ij \rangle\rangle} \hat{\mathbf{S}}_i \cdot \hat{\mathbf{S}}_j + \sum_{\langle\langle ij \rangle\rangle} \mathbf{D}_{ij} \cdot \hat{\mathbf{S}}_i \times \hat{\mathbf{S}}_j - h \sum_i \hat{S}_i^z, \quad (1)$$

where the first two terms are Heisenberg model with the nearest-neighbor (NN) and the next-nearest-neighbor

(NNN) ferromagnetic coupling, i.e., $J, J' > 0$. The third term is the out-of-plane NNN Dzyaloshinskii-Moriya interaction with $\mathbf{D}_{ij} = \nu_{ij} D \hat{\mathbf{z}}$, where $\nu_{ij} = +1(-1)$ indicates clockwise(counterclockwise) hopping. The last term is a Zeeman field with strength $h = g\mu_B B$, where g is the spin g factor and μ_B is the Bohr magneton. Because of the presence of the Zeeman field, the magnons are no longer protected by the Goldstone theorem and the spectrum are gapped at the Γ point [22]. Furthermore, the out-of-plane Zeeman field tends to align the localized spins along its direction as depicted in Fig. 1(b).

We convert the spin operators in Eq. (1) into the magnon creation (\hat{c}^\dagger) and annihilation (\hat{c}) operators by using the Holstein-Primakoff (HP) transformations: $\hat{S}_x + i\hat{S}_y = \sqrt{2S} - \hat{c}^\dagger \hat{c}$, $\hat{S}_x - i\hat{S}_y = \hat{c}^\dagger \sqrt{2S} - \hat{c}$, and $\hat{S}_z = S - \hat{c}^\dagger \hat{c}$. In the low temperature limit, $2S \gg \langle \hat{n} \rangle = \langle \hat{c}^\dagger \hat{c} \rangle$, and the square roots can be expanded in powers of $1/\sqrt{S}$. Truncated to $S^{\frac{1}{2}}$, we obtain the noninteracting Hamiltonian in the momentum space,

$$\mathcal{H}_0 = \sum_{\mathbf{k}} \Psi_{\mathbf{k}}^\dagger H_0(\mathbf{k}) \Psi_{\mathbf{k}}, \quad (2)$$

where $\Psi_{\mathbf{k}}^\dagger = (\hat{a}_{\mathbf{k}}^\dagger \hat{b}_{\mathbf{k}}^\dagger)$ is a spinor denoting the degrees of freedom for the two sublattices and $H_0(\mathbf{k}) = h_0(\mathbf{k})\sigma_0 + h_x(\mathbf{k})\sigma_x - h_y(\mathbf{k})\sigma_y + h_z(\mathbf{k})\sigma_z$. Here, $h_0(\mathbf{k}) = v_0 - 2v_t \cos \phi p_{\mathbf{k}}$, $h_x(\mathbf{k}) = -v_s \text{Re}(\gamma_{\mathbf{k}})$, $h_y(\mathbf{k}) = -v_s \text{Im}(\gamma_{\mathbf{k}})$, and $h_z(\mathbf{k}) = 2v_t \sin \phi \rho_{\mathbf{k}}$. In the above expressions, $\gamma_{\mathbf{k}} \equiv \sum_{n=1}^3 e^{i\mathbf{k} \cdot \delta_n}$ with δ_n being the three NN vectors, $v_0 = 3v_s + 6v'_s + h$, $v_t = \sqrt{v_s'^2 + v_D^2}$, $v_s(v_s')/(v_D) = JS(J'S)/(DS)$, $\phi = \arctan(D/J')$, $p_{\mathbf{k}} = \sum_{n=1}^3 \cos(\mathbf{k} \cdot \zeta_n)$, and $\rho_{\mathbf{k}} = \sum_{n=1}^3 \sin(\mathbf{k} \cdot \zeta_n)$, where ζ_n are the three NNN vectors. Diagonalizing $H_0(\mathbf{k})$ in the noninteracting Hamiltonian, Eq. (2), we obtain the single-particle magnon energies,

$$\varepsilon_\alpha(\mathbf{k}) = h_0(\mathbf{k}) + \lambda \epsilon(\mathbf{k}), \quad (3)$$

where $\epsilon(\mathbf{k}) = \sqrt{h_x^2(\mathbf{k}) + h_y^2(\mathbf{k}) + h_z^2(\mathbf{k})}$ and $\lambda = 1(-1)$ for the up(down) band, $\alpha = u(\alpha = d)$. The corresponding wavefunction is given by

$$|\psi_\alpha(\mathbf{k})\rangle = \frac{1}{\sqrt{2}} \begin{pmatrix} \sqrt{1 + \lambda \frac{h_z(\mathbf{k})}{\epsilon(\mathbf{k})}} \\ \lambda e^{-i\Phi(\mathbf{k})} \sqrt{1 - \lambda \frac{h_z(\mathbf{k})}{\epsilon(\mathbf{k})}} \end{pmatrix}, \quad (4)$$

where $\Phi_{\mathbf{k}} = \arg[h_x(\mathbf{k}) + ih_y(\mathbf{k})]$. From Eq. (3), it is easy to see that the spectrum remains gapped at the Dirac points \mathbf{K}_\pm with the gaps being $2|h_z(\mathbf{K}_\pm)|$ as long as the DMI is nonzero.

The Berry curvature for each energy band can be computed by $\Omega_\alpha(\mathbf{k}) = \nabla_{\mathbf{k}} \times \langle \psi_\alpha(\mathbf{k}) | i \nabla_{\mathbf{k}} | \psi_\alpha(\mathbf{k}) \rangle$. Topological phases of the system is characterized by the Chern number, defined as the integration of the Berry curvature over the Brillouin zone (BZ), $C_\alpha = \frac{1}{2\pi} \int_{\text{BZ}} d^2k \Omega_{z,\alpha}(\mathbf{k})$. For

the up and down bands of the noninteracting Hamiltonian, the associated Chern numbers describing the topological phase of the system are -1 and +1, respectively. The thermal Hall conductivity is also related to the Berry curvature by the following expression derived in Ref. [16],

$$\kappa_{xy}(T) = -\frac{k_B^2 T}{(2\pi)^2 \hbar} \sum_{\alpha} \int_{BZ} d^2 k c_2(n_{\alpha}) \Omega_{z,\alpha}(\mathbf{k}), \quad (5)$$

where $n_{\alpha} = [e^{\beta \varepsilon_{\alpha}(\mathbf{k})} - 1]^{-1}$ is the Bose distribution function and $\beta = 1/k_B T$, $c_2(x) = (1+x)(\log \frac{1+x}{x})^2 - (\log x)^2 - 2\text{Li}_2(-x)$, and Li_2 is the dilogarithm. The sign of the thermal Hall conductivity is the same as that of the Chern number for the up band. To see this, one can first show that $\Omega_u(\mathbf{k}) = -\Omega_d(\mathbf{k})$ and $\Omega_{\alpha}(\mathbf{k})$ never changes sign in the Brillouin zone, and observe that $c_2(x)$ is a monotonic function of x . At the level of noninteracting Hamiltonian, the system is always in the same topological phase ($C_u = -1$, $C_d = +1$) and $\kappa_{xy}(T)$ stays negative [23] for all parameter regimes.

Next, we consider the next order in $S^{-\frac{1}{2}}$ of the HP transformation to obtain magnon-magnon interactions. Using the eigenstates of the single-particle Hamiltonian, the interacting part \mathcal{H}_{int} of the full Hamiltonian can be expressed as,

$$\begin{aligned} \mathcal{H}_{\text{int}} = & \frac{1}{4SN} \sum_{\{\mathbf{k}_i\}} \left[V_{1,\{\mathbf{k}_i\}} \hat{u}_{\mathbf{k}_1}^{\dagger} \hat{u}_{\mathbf{k}_2}^{\dagger} \hat{u}_{\mathbf{k}_3} \hat{u}_{\mathbf{k}_4} \right. \\ & + V_{2,\{\mathbf{k}_i\}} \hat{u}_{\mathbf{k}_1}^{\dagger} \hat{u}_{\mathbf{k}_2}^{\dagger} \hat{u}_{\mathbf{k}_3} \hat{d}_{\mathbf{k}_4} + V_{3,\{\mathbf{k}_i\}} \hat{u}_{\mathbf{k}_1}^{\dagger} \hat{u}_{\mathbf{k}_2}^{\dagger} \hat{d}_{\mathbf{k}_3} \hat{d}_{\mathbf{k}_4} \\ & + V_{4,\{\mathbf{k}_i\}} \hat{u}_{\mathbf{k}_1}^{\dagger} \hat{d}_{\mathbf{k}_2}^{\dagger} \hat{u}_{\mathbf{k}_3} \hat{u}_{\mathbf{k}_4} + V_{5,\{\mathbf{k}_i\}} \hat{u}_{\mathbf{k}_1}^{\dagger} \hat{d}_{\mathbf{k}_2}^{\dagger} \hat{u}_{\mathbf{k}_3} \hat{d}_{\mathbf{k}_4} \quad (6) \\ & + V_{6,\{\mathbf{k}_i\}} \hat{u}_{\mathbf{k}_1}^{\dagger} \hat{d}_{\mathbf{k}_2}^{\dagger} \hat{d}_{\mathbf{k}_3} \hat{d}_{\mathbf{k}_4} + V_{7,\{\mathbf{k}_i\}} \hat{d}_{\mathbf{k}_1}^{\dagger} \hat{d}_{\mathbf{k}_2}^{\dagger} \hat{u}_{\mathbf{k}_3} \hat{u}_{\mathbf{k}_4} \\ & \left. + V_{8,\{\mathbf{k}_i\}} \hat{d}_{\mathbf{k}_1}^{\dagger} \hat{d}_{\mathbf{k}_2}^{\dagger} \hat{u}_{\mathbf{k}_3} \hat{d}_{\mathbf{k}_4} + V_{9,\{\mathbf{k}_i\}} \hat{d}_{\mathbf{k}_1}^{\dagger} \hat{d}_{\mathbf{k}_2}^{\dagger} \hat{d}_{\mathbf{k}_3} \hat{d}_{\mathbf{k}_4} \right] \\ & \delta_{-\mathbf{k}_1 - \mathbf{k}_2 + \mathbf{k}_3 + \mathbf{k}_4, 0}, \end{aligned}$$

where $\{\mathbf{k}_i\} = \{\mathbf{k}_1, \mathbf{k}_2, \mathbf{k}_3, \mathbf{k}_4\}$ and N is the total number of sublattice sites. \mathcal{H}_{int} is expressed in the ud basis related to the ab basis by the relation $(\hat{u}_{\mathbf{k}} \hat{d}_{\mathbf{k}})^T = P^{\dagger}(\hat{a}_{\mathbf{k}} \hat{b}_{\mathbf{k}})^T$, where P is the unitary transformation matrix associated with Eq. (4). The process of obtaining $V_{1,\{\mathbf{k}_i\}}$ to $V_{9,\{\mathbf{k}_i\}}$ is given in the supplementary material. To properly take into account many-body correlation effects from the magnon-magnon interactions, we employ the standard Green's function technique to determine the first order self-energy and from which we obtain renormalized energy spectrums. The self-energy we consider here is of the Hartree type and the corresponding Feynman diagram is shown in Fig. 1(c) [28]. The self-energy can be expressed as,

$$\Sigma_{\alpha\gamma}^{(1)}(\mathbf{k}, T) = \frac{1}{4SN\hbar} \sum_{\mathbf{q}, \lambda} S_{\alpha\gamma}^{\lambda}(\mathbf{k}, \mathbf{q}) n_{\lambda}(\mathbf{q}, T), \quad (7)$$

where α and γ represent either the up (u) or down (d) mode and $S_{\alpha\gamma}^{\lambda}(\mathbf{k}, \mathbf{q})$ is a function of momenta \mathbf{k} and \mathbf{q} . It

is understood from the Feynman diagram that the subscripts and the momentum of the self-energy correspond to those of the external Green's functions. The derivation of the self-energy and the explicit forms of $S_{\alpha\gamma}^{\lambda}$ can be found in the supplementary material.

Our next step follows from the Dyson's equation, $\mathcal{G}^{-1}(\mathbf{k}, \omega) = i\omega - \hbar^{-1}\varepsilon(\mathbf{k}) - \Sigma(\mathbf{k}, \omega)$, where \mathcal{G}^{-1} is the inverse of the dressed Green's function, ω is the bosonic Matsubara frequency, $\varepsilon(\mathbf{k})$ is the diagonalized matrix of H_0 in Eq. (2), and $\Sigma(\mathbf{k}, \omega)$ is the self-energy matrix. It suggests that the effect of \mathcal{H}_{int} can be integrated into an effective single-particle Hamiltonian by adding the contribution from the self-energy, given in Eq. (7), to \mathcal{H}_0 . That is,

$$\mathcal{H}_{\text{eff}} = \sum_{\mathbf{k}} \begin{pmatrix} \hat{u}_{\mathbf{k}}^{\dagger} & \hat{d}_{\mathbf{k}}^{\dagger} \end{pmatrix} \begin{pmatrix} \varepsilon_{\mathbf{k}}^u + \hbar\Sigma_{uu}^{(1)} & \hbar\Sigma_{ud}^{(1)} \\ \hbar\Sigma_{du}^{(1)} & \varepsilon_{\mathbf{k}}^d + \hbar\Sigma_{dd}^{(1)} \end{pmatrix} \begin{pmatrix} \hat{u}_{\mathbf{k}} \\ \hat{d}_{\mathbf{k}} \end{pmatrix}. \quad (8)$$

By directly diagonalizing the above effective Hamiltonian, we obtain the renormalized energy bands arising from the many-body correlation. We note here that when evaluating the thermal Hall conductivity, one needs to transform \mathcal{H}_{eff} back to the original ab basis as in Eq. (2): $\mathcal{H}_{\text{eff}} = \sum_{\mathbf{k}} \Psi_{\mathbf{k}}^{\dagger} H_{\text{eff}}(\mathbf{k}) \Psi_{\mathbf{k}}$. There are some intriguing phenomena occurred as a consequence of incorporating the first-order self energy. One of the major results in the paper is the recovery of the sign reversal of thermal Hall conductivity when the magnon-magnon interactions are included. Below we shall present and discuss our theoretical results in detail.

Results and discussion.—In this work, the following parameters are fixed: $S = \frac{1}{2}$ and $J' = D = 0.1J$. In Fig. 2(a), we plot the dispersion relations at three different temperatures when $h = 0.1J$. As can be seen from Eq. (7), the contribution from the self-energy vanishes at $T = 0$ because the Bose function for nonzero energies at low temperature approaches zero. As a result, the renormalized energies at $T = 0$ are the same as bare energies at the unperturbed level reported in Ref. [22]. As we increase the temperature, the gap at the Dirac point K_+ decreases and the spectrum becomes gapless at $T \approx J$ for this particular h . If we further increase the temperature, the gap opens up again and its size increases with T . Note here that the energy at Γ is given by h and is independent of the temperature. This is because the Zeeman interaction only couples to the \hat{S}_z term in Eq. (1) and the magnon-magnon interaction arising from the expansion of HP transformation for \hat{S}_z does not exist.

To see the temperature dependence of the gap, we extract the gap at K_+ for three different Zeeman energies as shown in Fig. 2(b). We find that as h increases, the gap-closing temperature T_c also increases. Although only the gap at K_+ is shown, it is in fact the same as the gap at K_- because of the inversion symmetry. It is straightforward to explicitly show that our model Hamiltonian at both perturbed and unperturbed level

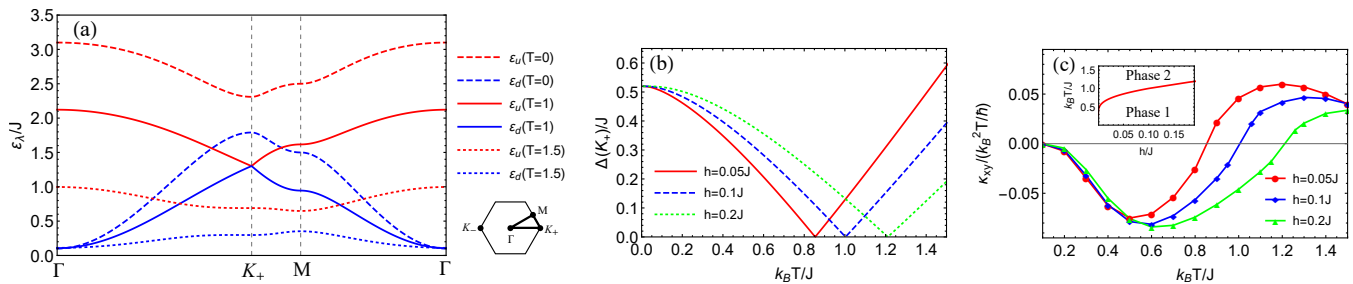


Figure 2. (a) Magnonic bandstructures for different temperatures along the path $\Gamma - K_+ - M - \Gamma$ as specified in the diagram of Brillouin zone next to the panel. Here K_+ is a Dirac point. The strength of the Zeeman field is $h = 0.1\text{J}$. (b) The gap Δ at the Dirac point K_+ as a function of temperature for three different strengths of the Zeeman field. (c) The thermal Hall conductivity vs temperature for the same Zeeman fields as in panel (b). The connecting lines are guides to the eyes. The inset shows the phase diagram as a function of temperature and Zeeman field. The Chern number $C_u = -1(+1)$ and $C_d = +1(-1)$ for phase 1 (phase 2).

possesses the inversion symmetry by examining the relation $\sigma_x H(-\mathbf{k}) \sigma_x = H(\mathbf{k})$ where $H = H_0$ or $H = H_{\text{eff}}$. The details are omitted. In addition, one can also draw the same conclusion from the fact that the magnetic field we consider here is out-of-plane and does not break the inversion symmetry. On the other hand, the time reversal symmetry condition $H^*(-\mathbf{k}) = H(\mathbf{k})$ does not hold because of the presence of DMI. Consequently, the energy differences between the up and down magnonic bands at two Dirac points are identical but the gapless feature is no longer protected.

We next turn to the discussion of thermal Hall conductivity. The gap reopens at a finite temperature suggests that there may be topological phase transitions at the critical temperature T_c . To confirm this, we compute the Chern numbers for both bands above and below T_c and verify that they indeed change sign at T_c . For definiteness, we plot in the inset of Fig. 2(c) the phase boundary between two distinct topological phases where the Chern numbers in phase 1 (phase 2) for the up and down bands are $C_u = -1(+1)$ and $C_d = +1(-1)$, respectively. The phase boundary in the h - T phase diagram can be determined by studying the gap at K_{\pm} as in Fig. 2(b). We note here that the signs of Berry curvatures at K_{\pm} change simultaneously due to the inversion symmetry in contrast to the Haldane model [25] with a nonzero onsite energy.

As discussed earlier, the topological phase transition can be experimentally confirmed from the sign reversal of thermal Hall conductivity κ_{xy} . Owing to the two-band property, one can directly associate the thermal Hall conductivity in Eq. (5) to $\Omega_u(\mathbf{k})$. In addition, we have checked numerically that $\Omega_u(\mathbf{k})$ has the same sign as the Chern number C_u for all \mathbf{k} in the Brillouin zone. From the fact that $c_2(x)$ is a monotonic function of x , one can deduce that the thermal Hall conductivity changes sign when the magnonic system of honeycomb lattices undergoes topological phase transitions. This is *distinct* from the thermal Hall conductivity of Kagome lattice. There, the topological phase transitions do not necessar-

ily cause the sign reversal of the thermal Hall conductivity. In Fig. 2(c), we plot κ_{xy} as functions of T for the same three Zeeman interaction as in Fig. 2(b). One can easily see that κ_{xy} evolves continuously with T and goes from being negative at low T ($T < T_c$) to being positive at high T ($T > T_c$). Here, we provide evidences that the sign reversal of the transport quantity is clearly a strong indication for topological phase transitions. This also makes the platform of honeycomb ferromagnet a good candidate for observing topological phase transitions in bosonic systems.

From the topological point of view, the DMI plays an essential role as opening up a gap for the magnonic bands. These non-crossings are the origin of a nonzero and well-defined Berry curvature and lead to nonzero topological invariants, i.e., Chern numbers. It is similar to the role of a spin-orbit interaction in the electronic topological insulators [29]. The major difference here is that the thermal Hall conductivity is not quantized as in quantum Hall effect because of the quantum statistics of magnons. Nevertheless, the sign of thermal Hall conductivity also has a topological origin as in the integers for quantized Hall conductance.

Conclusion.—To summarize, if magnon-magnon interactions are neglected, the system stays in the same topological phase ($C_u = -1, C_d = +1$) and the thermal Hall conductivity is always negative. However, when incorporating the Hartree-type self-energy arising from magnon-magnon interactions into the single-particle Hamiltonian, the system possesses two topological phases, ($C_u = -1, C_d = +1$) and ($C_u = +1, C_d = -1$). The topological phase of the system can be tuned either by temperature or external magnetic field and the corresponding phase transitions are driven by these magnon-magnon interactions. The sign of thermal Hall conductivity directly reflects the sign of the Chern numbers that characterize the topological phase. Therefore, the reversal of the sign for thermal Hall conductivity occurs during topological phase transitions and can serve as an indicator in future

experiments.

This work is supported by MOST Grant No. 108-2112-M-009-004-MY3.

(2010).

-
- [1] C. L. Kane and E. J. Mele, *Phys. Rev. Lett.* **95**, 226801 (2005).
 - [2] B. A. Bernevig and S.-C. Zhang, *Phys. Rev. Lett.* **96**, 106802 (2006).
 - [3] C. L. Kane and E. J. Mele, *Phys. Rev. Lett.* **95**, 146802 (2005).
 - [4] S. de Léséleuc, V. Lienhard, P. Scholl, D. Barredo, S. Weber, N. Lang, H. P. Büchler, T. Lahaye, and A. Browaeys, *Science* **365**, 775 (2019).
 - [5] K. H. Lee, S. B. Chung, K. Park, and J.-G. Park, *Phys. Rev. B* **97**, 180401 (2018).
 - [6] R. Seshadri and D. Sen, *Phys. Rev. B* **97**, 134411 (2018).
 - [7] Y. Ferreira and M. A. H. Vozmediano, *Phys. Rev. B* **97**, 054404 (2018).
 - [8] V. A. Zyuzin and A. A. Kovalev, *Phys. Rev. B* **97**, 174407 (2018).
 - [9] B. Li and A. A. Kovalev, *Phys. Rev. B* **97**, 174413 (2018).
 - [10] S. A. Owerre, *Journal of Physics: Condensed Matter* **30**, 245803 (2018).
 - [11] D. Bhowmick and P. Sengupta, *Phys. Rev. B* **101**, 195133 (2020).
 - [12] Y.-H. Li and R. Cheng, *Phys. Rev. B* **103**, 014407 (2021).
 - [13] S. A. Owerre, *Scientific Reports* **8**, 4431 (2018).
 - [14] S. Banerjee, D. S. L. Abergel, H. Ågren, G. Aeppli, and A. V. Balatsky, *Journal of Physics: Condensed Matter* **32**, 405603 (2020).
 - [15] H. Lee, J. H. Han, and P. A. Lee, *Phys. Rev. B* **91**, 125413 (2015).
 - [16] R. Matsumoto and S. Murakami, *Phys. Rev. Lett.* **106**, 197202 (2011).
 - [17] H. Katsura, N. Nagaosa, and P. A. Lee, *Phys. Rev. Lett.* **104**, 066403 (2010).
 - [18] Y. Onose, T. Ideue, H. Katsura, Y. Shiomi, N. Nagaosa, and Y. Tokura, *Science* **329**, 297 (2010).
 - [19] M. Hirschberger, R. Chisnell, Y. S. Lee, and N. P. Ong, *Phys. Rev. Lett.* **115**, 106603 (2015).
 - [20] A. Mook, J. Henk, and I. Mertig, *Phys. Rev. B* **89**, 134409 (2014).
 - [21] A. Mook, J. Henk, and I. Mertig, *Phys. Rev. B* **90**, 024412 (2014).
 - [22] S. A. Owerre, *Journal of Physics: Condensed Matter* **28**, 386001 (2016).
 - [23] S. A. Owerre, *Journal of Applied Physics* **120**, 043903 (2016).
 - [24] F. A. Gómez Albarracín, H. D. Rosales, and P. Pujol, *Phys. Rev. B* **103**, 054405 (2021).
 - [25] F. D. M. Haldane, *Phys. Rev. Lett.* **61**, 2015 (1988).
 - [26] S. K. Kim, H. Ochoa, R. Zarzuela, and Y. Tserkovnyak, *Phys. Rev. Lett.* **117**, 227201 (2016).
 - [27] S. S. Pershoguba, S. Banerjee, J. C. Lashley, J. Park, H. Ågren, G. Aeppli, and A. V. Balatsky, *Phys. Rev. X* **8**, 011010 (2018).
 - [28] L. Chen, J.-H. Chung, B. Gao, T. Chen, M. B. Stone, A. I. Kolesnikov, Q. Huang, and P. Dai, *Phys. Rev. X* **8**, 041028 (2018).
 - [29] M. Z. Hasan and C. L. Kane, *Rev. Mod. Phys.* **82**, 3045

Supplementary Material: Topological Phase transitions of Dirac Magnons in Honeycomb Ferromagnets

Yu-Shan Lu,¹ Jian-Lin Li,¹ and Chien-Te Wu^{1,2}

¹*Department of Electrophysics, National Yang Ming Chiao Tung University, Hsinchu, Taiwan*

²*Physics Division, National Center for Theoretical Sciences, Taipei, Taiwan*

A. COEFFICIENTS OF MAGNON-MAGNON INTERACTION

In deriving the first-order self-energy, we take advantage of the orthonormal relation in the ud basis to considerably simplify the process. In this section, we first derive the coefficients of the two-particle interacting Hamiltonian, \mathcal{H}_{int} , in Eq. (6) of the main text. Because there are 112 terms in total to deal with, the procedure is quite lengthy even though the principle behind the derivation is quite simple.

Using the Holstein-Primakoff (HP) transformation to expand the original Hamiltonian to the order of $S^{-\frac{1}{2}}$, we obtain the two-particle interacting Hamiltonian in the original ab basis

$$\begin{aligned} \mathcal{H}_{\text{int}} = & \frac{v_s}{4SN} \sum_{\{\mathbf{k}_i\}} \left(\gamma_{\mathbf{k}_4 - \mathbf{k}_1 - \mathbf{k}_2} \hat{b}_{\mathbf{k}_1}^\dagger \hat{b}_{\mathbf{k}_2}^\dagger \hat{a}_{\mathbf{k}_3} \hat{b}_{\mathbf{k}_4} + \gamma_{-\mathbf{k}_2} \hat{a}_{\mathbf{k}_1}^\dagger \hat{b}_{\mathbf{k}_2}^\dagger \hat{a}_{\mathbf{k}_3} \hat{a}_{\mathbf{k}_4} + \gamma_{\mathbf{k}_3} \hat{a}_{\mathbf{k}_1}^\dagger \hat{a}_{\mathbf{k}_2}^\dagger \hat{b}_{\mathbf{k}_3} \hat{a}_{\mathbf{k}_4} + \gamma_{-\mathbf{k}_1 + \mathbf{k}_4 + \mathbf{k}_3} \hat{b}_{\mathbf{k}_1}^\dagger \hat{a}_{\mathbf{k}_2}^\dagger \hat{b}_{\mathbf{k}_3} \hat{b}_{\mathbf{k}_4} \right. \\ & \left. - 4\gamma_{-\mathbf{k}_2 + \mathbf{k}_4} \hat{a}_{\mathbf{k}_1}^\dagger \hat{b}_{\mathbf{k}_2}^\dagger \hat{a}_{\mathbf{k}_3} \hat{b}_{\mathbf{k}_4} \right) \delta_{-\mathbf{k}_1 - \mathbf{k}_2 + \mathbf{k}_3 + \mathbf{k}_4, 0} \\ & + \frac{1}{4SN} \sum_{\{\mathbf{k}_i\}} \left\{ [v_t (\cos \phi \mathcal{P}_{\{\mathbf{k}_i\}} - \sin \phi \mathcal{Q}_{\{\mathbf{k}_i\}}) - 4v'_s p_{\mathbf{k}_4 - \mathbf{k}_2}] \hat{a}_{\mathbf{k}_1}^\dagger \hat{a}_{\mathbf{k}_2}^\dagger \hat{a}_{\mathbf{k}_3} \hat{a}_{\mathbf{k}_4} \right. \\ & \left. + [v_t (\cos \phi \mathcal{P}_{\{\mathbf{k}_i\}} + \sin \phi \mathcal{Q}_{\{\mathbf{k}_i\}}) - 4v'_s p_{\mathbf{k}_4 - \mathbf{k}_2}] \hat{b}_{\mathbf{k}_1}^\dagger \hat{b}_{\mathbf{k}_2}^\dagger \hat{b}_{\mathbf{k}_3} \hat{b}_{\mathbf{k}_4} \right\} \delta_{-\mathbf{k}_1 - \mathbf{k}_2 + \mathbf{k}_3 + \mathbf{k}_4, 0}, \end{aligned} \quad (\text{S1})$$

where $\mathcal{P}_{\{\mathbf{k}_i\}} \equiv p_{\mathbf{k}_1 + \mathbf{k}_2 - \mathbf{k}_4} + p_{\mathbf{k}_4 + \mathbf{k}_3 - \mathbf{k}_1} + p_{\mathbf{k}_2} + p_{\mathbf{k}_3}$ and $\mathcal{Q}_{\{\mathbf{k}_i\}} \equiv \rho_{\mathbf{k}_1 + \mathbf{k}_2 - \mathbf{k}_4} + \rho_{\mathbf{k}_4 + \mathbf{k}_3 - \mathbf{k}_1} + \rho_{\mathbf{k}_2} + \rho_{\mathbf{k}_3}$. In order to use the orthonormal relations in the ud basis, we transform the two-particle interaction from the ab basis to the ud basis with the following relations,

$$\hat{a}_{\mathbf{k}} = \frac{1}{\sqrt{2}} \left(A_{\mathbf{k}} \hat{u}_{\mathbf{k}} + M_{\mathbf{k}} \hat{d}_{\mathbf{k}} \right), \quad (\text{S2})$$

$$\hat{b}_{\mathbf{k}} = \frac{e^{-i\Phi_{\mathbf{k}}}}{\sqrt{2}} \left(M_{\mathbf{k}} \hat{u}_{\mathbf{k}} - A_{\mathbf{k}} \hat{d}_{\mathbf{k}} \right), \quad (\text{S3})$$

where $A_{\mathbf{k}} \equiv \sqrt{1 + \frac{\hbar_z(\mathbf{k})}{\epsilon(\mathbf{k})}}$ and $M_{\mathbf{k}} \equiv \sqrt{1 - \frac{\hbar_z(\mathbf{k})}{\epsilon(\mathbf{k})}}$. Substituting Eqs. (S2) and (S3) into Eq. (S1), one can derive the explicit forms of $V_{1, \{\mathbf{k}_i\}}$ to $V_{9, \{\mathbf{k}_i\}}$ defined in the main text.

B. COEFFICIENTS OF THE FIRST-ORDER SELF-ENERGY

The first-order self-energy can be expressed as $\Sigma_{\alpha\gamma}^{(1)}(\mathbf{k}, T) = \frac{1}{4SN\hbar} \sum_{\mathbf{q}} S_{\alpha\gamma}^u(\mathbf{k}, \mathbf{q}) n_u + S_{\alpha\gamma}^d(\mathbf{k}, \mathbf{q}) n_d$. Due to the orthonormal relation, it can be shown that $V_{3, \{\mathbf{k}\}}$ and $V_{7, \{\mathbf{k}\}}$ do not contribute to the first-order Green's function. Moreover, the three contractions yields three Kronecker deltas, which get rid of three momentum sums. The following

are the forms of $S_{\alpha\gamma}^\lambda(\mathbf{k}, \mathbf{q})$:

$$\left\{ \begin{array}{l} S_{uu}^u(\mathbf{k}, \mathbf{q}) = \frac{1}{4SN\hbar} [V_1(\mathbf{k}_1 = \mathbf{k}_4 = \mathbf{k}; \mathbf{k}_2 = \mathbf{k}_3 = \mathbf{q}) + V_1(\mathbf{k}_1 = \mathbf{k}_3 = \mathbf{k}; \mathbf{k}_2 = \mathbf{k}_4 = \mathbf{q}) \\ \quad + V_1(\mathbf{k}_2 = \mathbf{k}_4 = \mathbf{k}; \mathbf{k}_1 = \mathbf{k}_3 = \mathbf{q}) + V_1(\mathbf{k}_2 = \mathbf{k}_3 = \mathbf{k}; \mathbf{k}_1 = \mathbf{k}_4 = \mathbf{q})] \\ S_{uu}^d(\mathbf{k}, \mathbf{q}) = \frac{1}{4SN\hbar} [V_5(\mathbf{k}_1 = \mathbf{k}_3 = \mathbf{k}; \mathbf{k}_2 = \mathbf{k}_4 = \mathbf{q})] \\ S_{ud}^u(\mathbf{k}, \mathbf{q}) = \frac{1}{4SN\hbar} [V_2(\mathbf{k}_2 = \mathbf{k}_4 = \mathbf{k}; \mathbf{k}_1 = \mathbf{k}_3 = \mathbf{q}) + V_2(\mathbf{k}_1 = \mathbf{k}_4 = \mathbf{k}; \mathbf{k}_2 = \mathbf{k}_3 = \mathbf{q})] \\ S_{ud}^d(\mathbf{k}, \mathbf{q}) = \frac{1}{4SN\hbar} [V_6(\mathbf{k}_1 = \mathbf{k}_4 = \mathbf{k}; \mathbf{k}_2 = \mathbf{k}_3 = \mathbf{q}) + V_6(\mathbf{k}_1 = \mathbf{k}_3 = \mathbf{k}; \mathbf{k}_2 = \mathbf{k}_4 = \mathbf{q})] \\ S_{du}^u(\mathbf{k}, \mathbf{q}) = \frac{1}{4SN\hbar} [V_4(\mathbf{k}_2 = \mathbf{k}_4 = \mathbf{k}; \mathbf{k}_1 = \mathbf{k}_3 = \mathbf{q}) + V_4(\mathbf{k}_2 = \mathbf{k}_3 = \mathbf{k}; \mathbf{k}_1 = \mathbf{k}_4 = \mathbf{q})] \\ S_{du}^d(\mathbf{k}, \mathbf{q}) = \frac{1}{4SN\hbar} [V_8(\mathbf{k}_2 = \mathbf{k}_3 = \mathbf{k}; \mathbf{k}_1 = \mathbf{k}_4 = \mathbf{q}) + V_8(\mathbf{k}_1 = \mathbf{k}_3 = \mathbf{k}; \mathbf{k}_2 = \mathbf{k}_4 = \mathbf{q})] \\ S_{dd}^u(\mathbf{k}, \mathbf{q}) = \frac{1}{4SN\hbar} [V_5(\mathbf{k}_2 = \mathbf{k}_4 = \mathbf{k}; \mathbf{k}_1 = \mathbf{k}_3 = \mathbf{q})] \\ S_{dd}^d(\mathbf{k}, \mathbf{q}) = \frac{1}{4SN\hbar} [V_9(\mathbf{k}_2 = \mathbf{k}_4 = \mathbf{k}; \mathbf{k}_1 = \mathbf{k}_3 = \mathbf{q}) + V_9(\mathbf{k}_2 = \mathbf{k}_3 = \mathbf{k}; \mathbf{k}_1 = \mathbf{k}_4 = \mathbf{q}) \\ \quad + V_9(\mathbf{k}_1 = \mathbf{k}_4 = \mathbf{k}; \mathbf{k}_2 = \mathbf{k}_3 = \mathbf{q}) + V_9(\mathbf{k}_1 = \mathbf{k}_3 = \mathbf{k}; \mathbf{k}_2 = \mathbf{k}_4 = \mathbf{q})] \end{array} \right. \quad (S4)$$

The explicit expressions of $S_{\alpha\gamma}^u$ and $S_{\alpha\gamma}^d$ in Eqs. (S4) are

$$\begin{aligned} 4SN\hbar S_{uu}^{u,d}(\mathbf{k}, T) = & 2 \left[-\frac{h_x(\mathbf{k})^2 + h_y(\mathbf{k})^2}{\epsilon(\mathbf{k})} \mp \frac{h_x(\mathbf{q})^2 + h_y(\mathbf{q})^2}{\epsilon(\mathbf{q})} \right] \\ & + 2v_s \left[\mp \text{Re}\{e^{i(\Phi_{\mathbf{q}} - \Phi_{\mathbf{k}})} \gamma_{\mathbf{k}-\mathbf{q}}\} \sqrt{1 - \frac{h_z(\mathbf{k})^2}{\epsilon(\mathbf{k})^2}} \sqrt{1 - \frac{h_z(\mathbf{q})^2}{\epsilon(\mathbf{q})^2}} - 3 \left(1 \mp \frac{h_z(\mathbf{k})h_z(\mathbf{q})}{\epsilon(\mathbf{k})\epsilon(\mathbf{q})} \right) \right] \\ & + 4 [v_t \cos \phi(p_{\mathbf{q}} + p_{\mathbf{k}}) - v'_s p_{\mathbf{k}-\mathbf{q}} - 3v'_s] \left(1 \pm \frac{h_z(\mathbf{k})h_z(\mathbf{q})}{\epsilon(\mathbf{k})\epsilon(\mathbf{q})} \right) \\ & + 4v_t \sin \phi(\rho_{\mathbf{q}} + \rho_{\mathbf{k}}) \left(-\frac{h_z(\mathbf{k})}{\epsilon(\mathbf{k})} \mp \frac{h_z(\mathbf{q})}{\epsilon(\mathbf{q})} \right), \end{aligned} \quad (S5)$$

$$\begin{aligned} 4SN\hbar S_{ud}^{u,d} = & 2 \frac{\sqrt{h_x(\mathbf{k})^2 + h_y(\mathbf{k})^2} h_z(\mathbf{k})}{\epsilon(\mathbf{k})} \pm 6v_s \sqrt{1 - \frac{h_z(\mathbf{k})^2}{\epsilon(\mathbf{k})^2}} \frac{h_z(\mathbf{q})}{\epsilon(\mathbf{q})} \\ & + 2v_s \left[\pm \frac{h_z(\mathbf{k})}{\epsilon(\mathbf{k})} \text{Re}\{e^{i(\Phi_{\mathbf{k}} - \Phi_{\mathbf{q}})} \gamma_{-\mathbf{k}+\mathbf{q}}\} \mp i \text{Im}\{e^{i(\Phi_{\mathbf{k}} - \Phi_{\mathbf{q}})} \gamma_{-\mathbf{k}+\mathbf{q}}\} \right] \sqrt{1 - \frac{h_z(\mathbf{q})^2}{\epsilon(\mathbf{q})^2}} \\ & + 4 \sqrt{1 - \frac{h_z(\mathbf{k})^2}{\epsilon(\mathbf{k})^2}} \left\{ -v_t \sin \phi(\rho_{\mathbf{k}} + \rho_{\mathbf{q}}) \pm \frac{h_z(\mathbf{q})}{\epsilon(\mathbf{q})} [v_t \cos \phi(p_{\mathbf{k}} + p_{\mathbf{q}}) - v'_s p_{\mathbf{k}-\mathbf{q}} - 3v'_s] \right\}, \end{aligned} \quad (S6)$$

$$S_{du}^{u,d} = (S_{ud}^{u,d})^*, \quad (S7)$$

$$\begin{aligned} 4SN\hbar S_{dd}^{u,d} = & 2 \left[\frac{h_x(\mathbf{k})^2 + h_y(\mathbf{k})^2}{\epsilon(\mathbf{k})} \mp \frac{h_x(\mathbf{q})^2 + h_y(\mathbf{q})^2}{\epsilon(\mathbf{q})} \right] + 2v_s \left[\pm \text{Re}\{e^{i(\Phi_{\mathbf{q}} - \Phi_{\mathbf{k}})} \gamma_{\mathbf{k}-\mathbf{q}}\} \sqrt{1 - \frac{h_z(\mathbf{k})^2}{\epsilon(\mathbf{k})^2}} \sqrt{1 - \frac{h_z(\mathbf{q})^2}{\epsilon(\mathbf{q})^2}} \right. \\ & \left. - 3 \left(1 \pm \frac{h_z(\mathbf{k})h_z(\mathbf{q})}{\epsilon(\mathbf{k})\epsilon(\mathbf{q})} \right) \right] + 4 [v_t \cos \phi(p_{\mathbf{q}} + p_{\mathbf{k}}) - v'_s p_{\mathbf{k}-\mathbf{q}} - 3v'_s] \left(1 \mp \frac{h_z(\mathbf{k})h_z(\mathbf{q})}{\epsilon(\mathbf{k})\epsilon(\mathbf{q})} \right) \\ & + 4v_t \sin \phi(\rho_{\mathbf{q}} + \rho_{\mathbf{k}}) \left[\frac{h_z(\mathbf{k})}{\epsilon(\mathbf{k})} \mp \frac{h_z(\mathbf{q})}{\epsilon(\mathbf{q})} \right], \end{aligned} \quad (S8)$$

where the upper and lower signs are for $S_{\alpha\gamma}^u$ and $S_{\alpha\gamma}^d$, respectively.

C. AVOID UNDEFINED PHASE IN THE EIGENSTATES FOR DIRAC POINTS

The phase in Eq. (S3) are not defined at two Dirac points in Brillouin zone (BZ) owing to the fact that $h_x(\mathbf{K}_{\pm}) = h_y(\mathbf{K}_{\pm}) = 0$. Therefore, one can not compute relevant physical quantities such as the self-energy and effective

Hamiltonian with this particular gauge. To resolve this problem, we divide the BZ into two regions, each one contains a single Dirac point. In the region containing \mathbf{K}_+ , we use

$$\begin{aligned}\hat{a}_{\mathbf{k}} &= \frac{1}{\sqrt{2}} \left(\frac{h_x(\mathbf{k}) + ih_y(\mathbf{k})}{\sqrt{\epsilon(\mathbf{k}) (\epsilon(\mathbf{k}) - h_z(\mathbf{k}))}} \hat{u}_{\mathbf{k}} + \sqrt{1 - \frac{h_z(\mathbf{k})}{\epsilon(\mathbf{k})}} \hat{d}_{\mathbf{k}} \right), \\ \hat{b}_{\mathbf{k}} &= \frac{1}{\sqrt{2}} \left(\sqrt{1 - \frac{h_z(\mathbf{k})}{\epsilon(\mathbf{k})}} \hat{u}_{\mathbf{k}} - \frac{h_x(\mathbf{k}) - ih_y(\mathbf{k})}{\sqrt{\epsilon(\mathbf{k}) (\epsilon(\mathbf{k}) - h_z(\mathbf{k}))}} \hat{d}_{\mathbf{k}} \right),\end{aligned}\tag{S9}$$

corresponding to a different gauge choice than Eq. (S3). While in the other region containing \mathbf{K}_- , we adopt another gauge to write down

$$\begin{aligned}\hat{a}_{\mathbf{k}} &= \frac{1}{\sqrt{2}} \left(\sqrt{1 + \frac{h_z(\mathbf{k})}{\epsilon(\mathbf{k})}} \hat{u}_{\mathbf{k}} - \frac{h_x(\mathbf{k}) + ih_y(\mathbf{k})}{\sqrt{\epsilon(\mathbf{k}) (\epsilon(\mathbf{k}) + h_z(\mathbf{k}))}} \hat{d}_{\mathbf{k}} \right), \\ \hat{b}_{\mathbf{k}} &= \frac{1}{\sqrt{2}} \left(\frac{h_x(\mathbf{k}) - ih_y(\mathbf{k})}{\sqrt{\epsilon(\mathbf{k}) (\epsilon(\mathbf{k}) + h_z(\mathbf{k}))}} \hat{u}_{\mathbf{k}} + \sqrt{1 + \frac{h_z(\mathbf{k})}{\epsilon(\mathbf{k})}} \hat{d}_{\mathbf{k}} \right).\end{aligned}\tag{S10}$$

Both Eq. (S9) and (S10) are used to perform momentum sums when evaluating physical quantities of interest. Although we use different gauges to compute the physical quantities, one can prove that the self-energy in the ab basis, effective Hamiltonian, energy bands, Berry curvature, and Hall conductivity are all gauge invariant.